Biochemical and Biophysical Research Communications 461 (2015) 487–493

Contents lists available at ScienceDirect

Biochemical and Biophysical Research Communications

journal homepage: www.elsevier.com/locate/ybbrc

Structural insight into the substrate inhibition mechanism of NADP$^+$-dependent succinic semialdehyde dehydrogenase from *Streptococcus pyogenes*

Eun Hyuk Jang [a], Seong Ah Park [b], Young Min Chi [a, *], Ki Seog Lee [b, **]

[a] Department of Biosystems and Biotechnology, College of Life Sciences and Biotechnology, Korea University, Seoul 136-713, Republic of Korea
[b] Department of Clinical Laboratory Science, College of Health Sciences, Catholic University of Pusan, Busan 609-757, Republic of Korea

ARTICLE INFO

Article history:
Received 31 March 2015
Available online 16 April 2015

Keywords:
Succinic semialdehyde dehydrogenase
Streptococcus pyogenes
Substrate inhibition
ESS-complex structure

ABSTRACT

Succinic semialdehyde dehydrogenases (SSADHs) are ubiquitous enzymes that catalyze the oxidation of succinic semialdehyde (SSA) to succinic acid in the presence of NAD(P)$^+$, and play an important role in the cellular mechanisms including the detoxification of accumulated SSA or the survival in conditions of limited nutrients. Here, we report the inhibitory properties and two crystal structures of SSADH from *Streptococcus pyogenes* (SpSSADH) in a binary (ES) complex with SSA as the substrate and a ternary (ESS) complex with the substrate SSA and the inhibitory SSA, at 2.4 Å resolution for both structures. Analysis of the kinetic inhibitory parameters revealed significant substrate inhibition in the presence of NADP$^+$ at concentrations of SSA higher than 0.02 mM, which exhibited complete uncompetitive substrate inhibition with the inhibition constant (K_i) value of 0.10 ± 0.02 mM. In ES-complex of SpSSADH, the SSA showed a tightly bound bent form nearby the catalytic residues, which may be caused by reduction of the cavity volume for substrate binding, compared with other SSADHs. Moreover, structural comparison of ESS-complex with a binary complex with NADP$^+$ of SpSSADH indicated that the substrate inhibition was induced by the binding of inhibitory SSA in the cofactor-binding site, instead of NADP$^+$. Our results provide first structure-based molecular insights into the substrate inhibition mechanism of SpSSADH as the Gram-positive bacterial SSADH.

1. Introduction

Aldehyde dehydrogenases (ALDHs) are a large group of enzymes that catalyze the oxidation of various aldehydes to the corresponding carboxylic acids in the presence of NAD(P)$^+$ [1]. These enzymes are found in all organisms including archaea, bacteria and eukaryotes, and play important roles in cellular metabolisms. Moreover, ALDHs are involved in the conversion of biomolecules and the modulation of cellular homeostasis, as well as in the detoxification of accumulated aldehydes derived from endogenous production and/or exogenous exposures [1,2].

Succinic semialdehyde dehydrogenase (SSADH) belongs to the ALDH superfamily and catalyzes the NAD(P)$^+$-dependent oxidation of succinic semialdhyde (SSA) to succinic acid (SA) in the final step of γ-aminobutyric acid (GABA) catabolism with strict substrate specificity for SSA [3]. GABA, as a ubiquitous non-protein amino acid in various organisms, is synthesized from glutamate by glutamate decarboxylase. GABA can be introduced into the tricarboxylic acid (TCA) cycle by a two-step reaction. First, GABA is converted by GABA transaminase to SSA, which is sequentially oxidized to SA by SSADH [4,5]. Mutations in the *ssadh* genes leading to defective SSA metabolism cause rare autosomal recessive diseases in human and induce various developmental and phenotypic changes in plants [3,6,7]. Hence, bacteria use SSADH in threatening conditions, such as accumulation of toxic SSA and limitation of nutrients for survival [5,8].

To date, molecular mechanisms of substrate inhibition have been proposed for several bacterial SSADHs [3,9], including the formation of a covalent adduct between the oxidized forms of substrate and cofactor, or substrate binding at an allosteric site [9–11], but the structure-based evidence has not been reported yet. Although our previous studies have suggested that SSADH from *Streptococcus pyogenes* (SpSSADH) prefers NADP$^+$ to NAD$^+$ as a

* Corresponding author. Fax: +82 2 921 3702.
** Corresponding author. Fax: +82 51 510 0568.
E-mail addresses: ezeg@korea.ac.kr (Y.M. Chi), kslee@cup.ac.kr (K.S. Lee).

http://dx.doi.org/10.1016/j.bbrc.2015.04.047
0006-291X/

hydride acceptor by analyses of the kinetic parameters and the binary complex structure with $NADP^+$ [12], the mechanism of substrate inhibition by SpSSADH remains still to be addressed. Here, we present the kinetic properties of substrate inhibition and two crystal structures of $NADP^+$-dependent SpSSADH, including a binary (ES) complex with SSA as a substrate and a ternary (ESS) complex with substrate SSA and inhibitory SSA, at 2.4 Å resolution for both structures. Analysis of the kinetic inhibitory parameters showed a significant substrate inhibition depending on the concentration of substrate SSA in the presence of $NADP^+$, and exhibited complete uncompetitive substrate inhibition at higher concentrations of SSA. Moreover, the crystal structure of ESS-complex indicated that the substrate inhibition of SpSSADH was induced by binding of inhibitory SSA into the cofactor-binding site, interfering with the binding of $NADP^+$ by torsion-angle change of Tyr188 side chain. Our results provide structure-based insightful information regarding the mechanism of substrate inhibition of SpSSADH.

2. Materials and methods

2.1. Preparation of SpSSADH enzyme

The preparation of SpSSADH enzyme, including expression and purification, was carried out as previously described [13]. Briefly, SpSSADH was expressed in transformed *Escherichia coli* BL21 (DE3) strain harboring cloned pET-28a vector with the gene encoding SSADH from *S. pyogenes*. Sequentially, overexpressed SpSSADH enzyme was purified using metal ion affinity chromatography and size-exclusion chromatography. Then, the purified enzyme was concentrated to 29.6 mg/ml and stored at −80 °C. The enzyme concentration was estimated using the Bradford assay, and the active enzyme molarity was determined by cysteine titration at the unfolded state using 5,5′-dithio*bis*(2-nitrobenzoate) (Sigma) [14].

2.2. Enzyme assay and kinetic analysis for substrate inhibition

For substrate inhibition assay of SpSSADH, the enzyme activities were measured with varying the concentrations of SSA as a substrate at a fixed concentration of $NADP^+$ by monitoring the increase of absorbance at UV 340 nm (ε_{340} 6.22 mM^{-1} cm^{-1}), resulting from the conversion of $NADP^+$ to NADPH. The reaction mixtures (1.0 ml), containing 20 mM Tris–HCl pH 7.0 and 5.0 mM DTT, were pre-incubated with 0.2 mM $NADP^+$ and various concentrations of SSA (0.005–0.6 mM) at 30 °C for 5 min. After pre-incubation of the reaction mixtures, the reaction was initiated by adding of SpSSADH (1 μg/ml, 0.0393 μM). The initial velocities were estimated from the initial linear portion for the time-courses. All reactions were performed in triplicate.

The kinetic parameters for substrate inhibition were determined by nonlinear least-square fitting to the substrate inhibition equation [15] using SigmaPlot ver. 10.0 and GraphPad Prism 6. Briefly, the equation for substrate inhibition, considering a non-productive binding of the substrate to the enzyme, is written as

$$V = \frac{V_{max}[S]}{K_m + [S] + [S]^2 / K_i} \quad (1)$$

, where $[S]$ is the concentration of substrate, V_{max} is the maximal velocity, K_m is the Michaelis constant for the substrate, and K_i is the

Table 1
Data collection and refinement statistics of SpSSADH.

	ES-complex	ESS-complex
PDB ID	4YWU	4YWV
Data collection		
Space group	$P4_32_12$	$P4_32_12$
Wavelength (Å)	0.97951	0.97951
Cell dimensions (Å)	$a = 134.965$, $b = 134.965$,$c = 172.551$	$a = 134.198$, $b = 134.198$,$c = 172.303$
Resolution range (Å)	50.0–2.4 (2.49–2.40)	50.0–2.4 (2.49–2.40)
Total reflections	438,032	219,294
Unique reflections	61,642	56,597
Completeness (%)	98.2 (95.4)	92.0 (85.8)
R_{merge}[a] (%)	16.5 (48.8)	11.0 (30.8)
Redundancy	7.1 (4.5)	3.9 (2.8)
$I/\sigma(I)$	10.9 (2.5)	14.8 (3.1)
Refinment		
Resolution range (Å)	42.7–2.4	41.6–2.4
R/R_{free}[b] (%)	21.3/25.3	20.1/24.5
No. of atoms		
Protein	7,148	7,148
Water	590	429
SSA	14	28
SO_4	20	15
Average *B*-factors		
Protein (Å^2)	33.9	33.3
Water (Å^2)	35.2	35.1
SSA (Å^2)	55.3	50.0
RMS deviations		
Bond length (Å)	0.006	0.007
Bond angle (°)	1.2	1.3
Ramachandran plot		
Favored (%)	99.4	99.3
Allowed (%)	0.6	0.7
Disallowed (%)	0	0

Values in parentheses indicate data of the highest resolution shell.
[a] $R_{merge} = \sum|I_h - \langle I_h\rangle| / \sum I_h$, where I_h represents the observed intensity and $\langle I_h\rangle$ is the average intensity.
[b] $R = \sum||F_{obs}| - |F_{calc}|| / \sum |F_{obs}|$, where $|F_{obs}|$ and $|F_{calc}|$ represent the observed and calculated structure factor amplitudes, respectively. R_{free} is calculated for a randomly chosen 5% of reflections, which were not used during refinement calculations.

Table 2
Steady-state kinetic parameters of SpSSADH.

Variable ligand	Fixed substrate	K_m (mM)	k_{cat} (s^{-1})	k_{cat}/K_m (M^{-1} s^{-1})	K_i (mM)	R^{2a}
SSA	$NADP^+$ (0.2 mM)	$3.95 \pm 0.08 \times 10^{-3}$	1.69 ± 0.47	$4.26 \pm 1.10 \times 10^{5}$	0.10 ± 0.02	0.9905

[a] R^2 = Coefficient of determination.

inhibitory constant independent of [*S*]. For determination of the parameters in Eq. (1), an individual saturation curve was analyzed by division into two sections depending on the concentration of substrate. In the low concentration range, the term $[S]^2/K_i$ is neglected and the equation is written as

$$V = \frac{V_{max}[S]}{K_m + [S]} \quad (2)$$

, which is the form of Michaelis–Menten kinetics, and K_m can be determined by the Lineweaver–Burk plot. Meanwhile, in the high concentration range, the term $K_m/[S]$ is neglected and Eq. (1) becomes

$$V = \frac{V_{max}K_i}{K_i + [S]} \quad (3)$$

, and a plot of 1/V versus [*S*] is used to determine V_{max} and K_i. In this way, using only a constrained part of the measured data, the three parameters in Eq. (1) can be evaluated.

2.3. Crystallization, data collection and structure determination

Prepared SpSSADH enzyme was crystallized at 22 °C using the hanging-drop vapor diffusion method by drop mixture of 1 μl protein solution with 1 μl reservoir solution. For ES-complex crystal, SpSSADH was pre-incubated with SSA at the molar ratio of 1:2, and the protein-substrate mixture was crystallized over 500 μl reservoir solution containing 0.1 M Sodium acetate trihydrate pH 4.6 and 2.0 M Ammonium sulfate. The crystal of ESS-complex was obtained by soaking the pre-grown NAD^+ co-crystallized crystal with a 1:10 molar ratio of SSA under the same reservoir conditions.

For data collection, both ES-complex and ESS-complex crystals were cryoprotected with 25% (v/v) ethylene glycol in reservoir solution. Then, both crystals were flash-frozen in a liquid nitrogen stream. X-ray diffraction data sets of both ES-complex and ESS-complex crystals were collected at 2.4 Å resolution on beamline 5C of Pohang Accelerator Laboratory (Pohang, South Korea) using an ADSC Quantum 315r CCD detector. All data sets were indexed, integrated and scaled using *HKL-2000* software package [16].

Initial structures of ES-complex and ESS-complex were solved by the molecular-replacement (MR) method using *PHENIX* program [17] with the apo-structure of SpSSADH (PDB ID 4OGD) [12] as the search model. Both structures belonged to the tetragonal $P4_32_12$ with one dimer per an asymmetric unit. The structural refinements including rigid body refinement and simulated annealing refinement were performed with *CNS* program [18], and the model was rebuilt using *COOT* [19]. The final model of ES-complex contained one SSA per each subunit, and the final values of R_{factor} and R_{free} were 21.3% and 25.3%, respectively. ESS-complex final model contained two SSA molecules per each subunit, with the final R_{factor} and R_{free} values of 20.1% and 24.5%, respectively. The data collection and final refinement statistics are summarized in Table 1. Structure validations of both structures were analyzed with *PROCHECK* program [20] and all structure figures were prepared using *PyMOL* [21].

2.4. Protein data bank accession number

The atomic coordinates and structure factors of ES-complex and ESS-complex structures have been deposited in the Protein Data

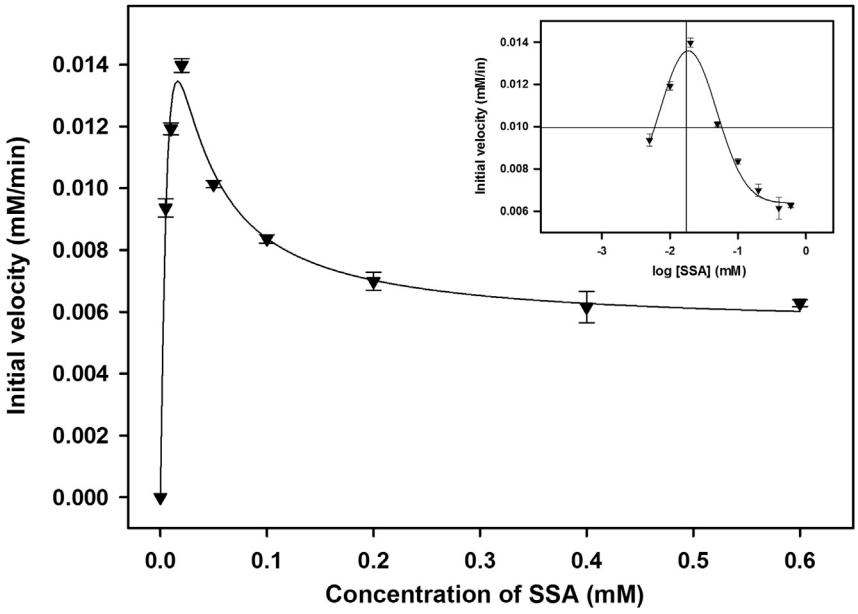

Fig. 1. Substrate inhibition of SpSSADH activity. The initial velocity curve for SpSSADH as a function of various concentrations of SSA (0.005–0.6 mM) is shown at a fixed concentration of $NADP^+$ (0.2 mM). The inset shows the data plotted as initial velocity versus the log of SSA concentration in the presence of $NADP^+$. The lines are drawn to highlight the symmetry, with the vertical line drawn at the apex of the curve and the horizontal line drawn at half-height of the curve.

Bank (http://www.rcsb.org/pdb) with accession numbers 4YWU and 4YWV, respectively.

3. Results and discussion

3.1. Catalytic properties of SpSSADH by substrate inhibition

Several enzymes including dehydrogenases, kinases, methyltransferases and hydroxylases are inhibited by their own substrates, leading to a velocity curve that rises to a maximum as the substrate concentration increases and then descends either to zero or to a non-zero asymptote [11]. This phenomenon is referred to as the substrate inhibition, and has been considered to be a relevant regulatory mechanism in several biological metabolic pathways [1]. Among such enzymes, several molecular mechanisms for substrate inhibition have been proposed for dehydrogenases, including the formation of a covalent adduct between the oxidized forms of substrate and cofactor, substrate binding at a second site away from the active site, and the formation of a nonproductive enzyme complex with the cofactor and/or substrate [1,9].

Our previous study on the cofactor preference of SpSSADH at a fixed concentration of SSA showed that no substrate inhibition was observed when NAD^+ or $NADP^+$ were used as substrates [12]. Thus, to elucidate the substrate inhibition mechanism of $NADP^+$-dependent SpSSADH, the initial velocities were estimated by varying the concentrations of SSA at a constant concentration of 0.2 mM $NADP^+$. As shown in Fig. 1, the reaction rate of SpSSADH reached quickly to maximum velocity in the lower range of SSA concentrations, but this trend was reversed at the higher SSA concentrations and the reaction velocity decreased as the SSA concentration was increased. It was therefore determined that SpSSADH showed the substrate inhibition phenomenon in the presence of $NADP^+$ at concentrations of SSA higher than 0.02 mM with the inhibition constant (K_i) values of 0.10 ± 0.02 mM (see Table 2). Moreover, the plot of initial velocity versus the log of SSA concentration (Fig. 2, inset) showed a symmetrical curve which approached complete inhibition at high substrate concentrations, as previously demonstrated in several microbial and human dehydrogenases [10,11,15]. This behavior is consistent with complete uncompetitive substrate inhibition [10], and the substrate concentration data fit well with Eq. (1) describing this type of inhibition.

3.2. Substrate binding site of SpSSADH

To investigate the substrate-binding mode, the crystal structure of SpSSADH in a binary (ES) complex with SSA was determined at 2.4 Å resolution with the $P4_32_12$ crystallographic space group. The

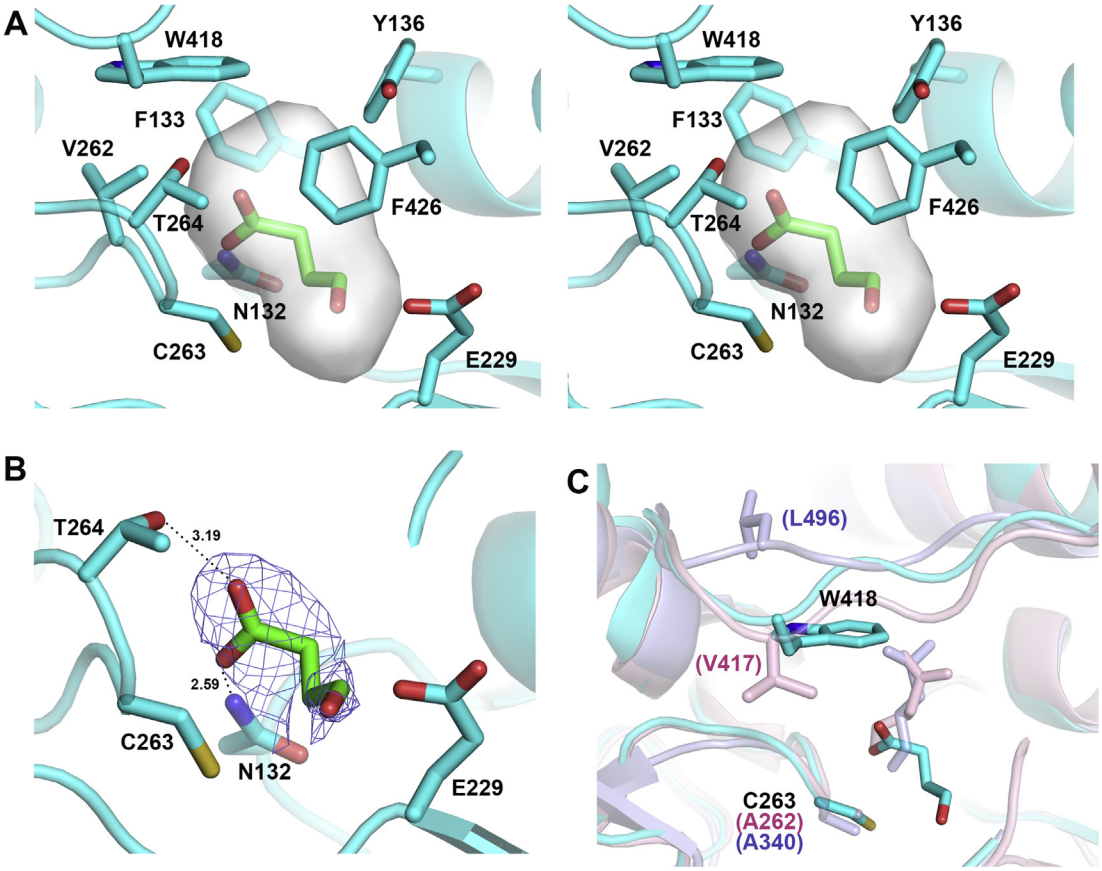

Fig. 2. The substrate-binding site of SpSSADH with SSA. (A) The substrate-binding pocket of SpSSADH. Stereo view of the active site of SpSSADH with SSA is shown in the cartoon model. The residues forming the substrate-binding pocket and SSA are shown in the stick model in cyan and green color, respectively. The substrate-binding pocket of ES-complex of SpSSADH is shown in buried surface representation with white color. (B) The substrate-binding model of SpSSADH. The active site of SpSSADH is shown in cartoon, and SSA as the substrate is represented in green color in the stick model. The catalytic residues and hydrogen bonds forming residues with SSA are shown in cyan color in the stick model. The blue-colored mesh describes the omitted $2F_o$-F_c electron density map for SSA at 0.8 σ. The hydrogen bond interactions are displayed by black dotted lines with distances. (C) Structural comparison of SpSSADH with other SSADHs at the substrate-binding site. ES-complex structure of SpSSADH is superimposed with the SSA-bound SSADH structures from human (PDB ID 2W8Q) and *Synechococcus* (PDB ID 3VZ3). SpSSADH, HsSSADH and SySSADH structures are shown in cyan, blue and pink, respectively. Trp418 and Cys263 including their corresponding residues are shown in stick model. The residues in SpSSADH are labeled with black characters, while their corresponding residues in HsSSADH and SySSADH are labeled in parentheses with blue and pink, respectively. (For interpretation of the references to color in this figure legend, the reader is referred to the web version of this article.)

overall structure of ES-complex did not significantly differ from the apo-structure (PDB ID 4OGD), with an RMSD of 0.65 Å. In the active site of SpSSADH, SSA was buried inside of the substrate-binding pocket formed by Phe133, Tyr136, Val262, Trp418 and Phe426 residues (Fig. 2A). While the position of the substrate was restricted by the cramped binding pocket with a cavity volume of 173 $Å^3$ (*CASTp*, [22]), the carboxyl group of SSA was stabilized by hydrogen bonds with the side chains of Asn132 and Thr264, and the aldehyde tail was located at between Cys263 and Glu229 as the catalytic residues (Fig. 2B).

Structural comparison for ES-complex of SpSSADH with that of other SSADHs showed slightly differences in the binding position of the substrate in the active site. Due to the relatively smaller size of the substrate-binding pocket, the SSA in SpSSADH showed a bent form nearby the catalytic residues, unlike the SSA that located as the stretched form at the active site in the binary complex structures of human SSADH (HsSSADH) or *Synechococcus* SSADH (SySSADH) (Fig. 2C). While most residues involved in the substrate-binding pocket are conserved in SpSSADH, Tyr136 and Trp418 residues are replaced from other SSADHs. Particularly, the residue, Trp418 containing a bulky side chain corresponding to Leu496 of HsSSADH and Val417 of SySSADH, may expect to affect the positioning of SSA while binding to SpSSADH. Namely, the side chain of Trp418 in SpSSADH is located closely to the carboxyl group of SSA, which may induce tighter binding ($3.95 \pm 0.08 \times 10^{-3}$ mM) of the substrate SSA into the active site, compared with other SSADHs (Fig. 2C). Thus, we assume that Trp418 of SpSSADH may contribute to the enhancement of the binding affinity for the substrate caused by the reduction of cavity volume for the substrate-binding pocket, although further studies still remain to elucidate its function.

3.3. Structural basis for substrate inhibition of SpSSADH

The molecular mechanisms of substrate inhibition have been proposed for several SSADHs, but structural evidence for the binding properties of inhibitory substrate has remained elusive. During the experiments to obtain a ternary complex of SpSSADH with the cofactor and SSA, the binary complex crystals with cofactor were soaked by higher concentrations of SSA, which may induce substrate inhibition. Fortunately, the ternary (ESS) complex crystals with substrate SSA and inhibitory SSA were obtained, and then ESS-complex structure was determined at a 2.4 Å resolution with the $P4_32_12$ crystallographic space group. In the ternary complex structure of SpSSADH, two molecules of SSA, acting as the substrate and inhibitor, were located in the active site and the cofactor-binding site, respectively, with stabilization through hydrogen bonding with neighboring residues, and clearly

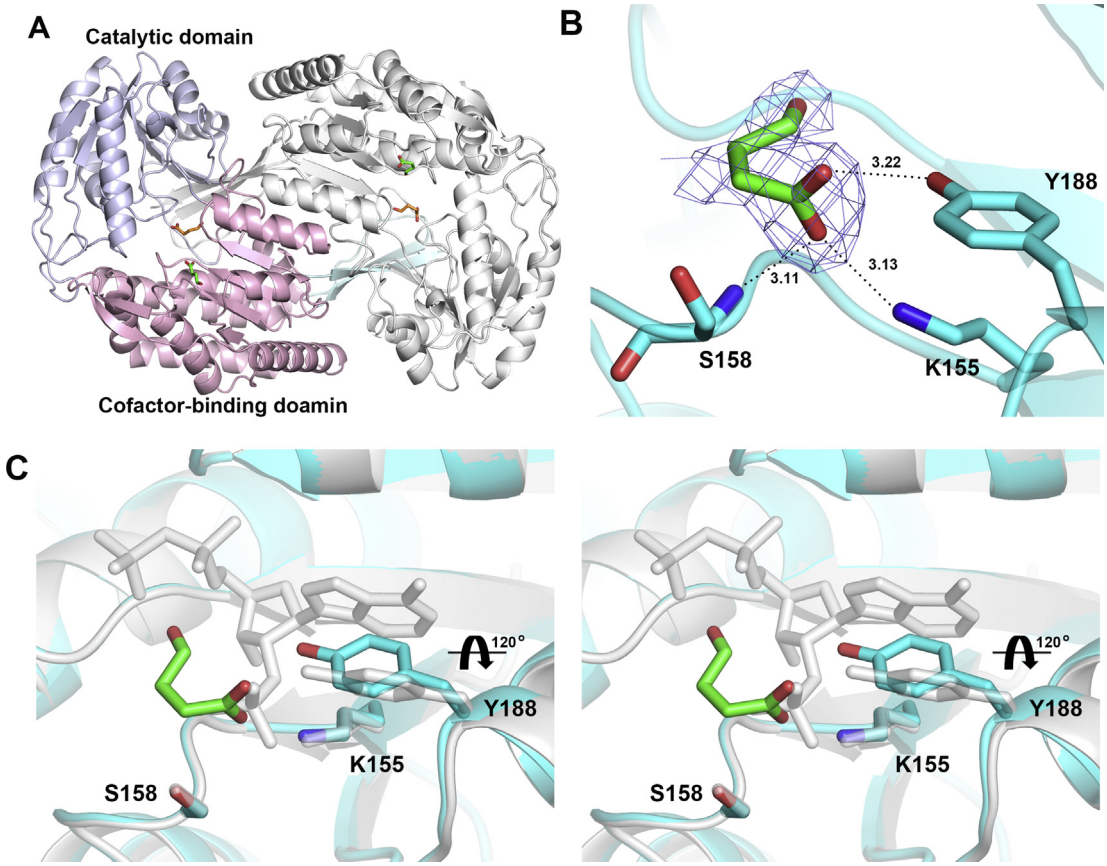

Fig. 3. The ternary complex (ESS) structure of SpSSADH. (A) Overall structure of SpSSADH dimer in complex with the substrate and inhibitory SSAs. The catalytic domain and the cofactor-binding domain of one subunit are colored in blue and pink, respectively. SSAs as the substrate are colored in orange and located in the catalytic loop. Inhibitory SSAs are represented with green color, and are located in the cofactor-binding site. (B) Inhibitory SSA in the cofactor-binding site. The inhibitory SSA of SpSSADH is located at the position of interaction of the 2′-phosphate group of the adenine-side ribose in $NADP^+$. Blue mesh represents the omitted $2F_o$-F_c electron density map for SSA as an inhibitor at 1.0 σ. The hydrogen bond-forming residues are shown in cyan color in the stick model. The hydrogen bond interactions are indicated by black dotted lines with distances. (C) Stereo view of the superimposed ESS-complex structure with the binary complex structure (PDB ID 4OHT) of SpSSADH containing $NADP^+$ as a cofactor. ESS-complex and binary complex structures are shown in cartoon model using cyan and white color, respectively. The inhibitory SSA and partial $NADP^+$ are represented in stick model with green and white color, respectively. The residues forming hydrogen bonds with the inhibitory SSA or the 2′-phosphate group of the adenine-side ribose in $NADP^+$ are shown in the stick model and labeled with black characters. (For interpretation of the references to color in this figure legend, the reader is referred to the web version of this article.)

confirmed using the omitted $2F_o$-F_c electron density map (Fig. 3A and B). Particularly, it was found that the carboxylic group of the inhibitory SSA in ESS-complex structure interacted with nearby Lys155, Ser158 and Tyr188 residues, which were involved in the stabilization of the 2′-phosphate group of the adenine-side ribose in $NADP^+$ (Fig. 3B). Besides, the orientation of the aldehyde tail of the inhibitory SSAs, which was bound to each subunit, exhibited the opposite direction on the ESS-complex structure, but the carboxyl groups of both inhibitory SSAs were located at similar position, and interacted with identical residues as mentioned above.

Structural superimposition of ESS-complex of SpSSADH with the binary complex (PDB ID 4OHT) containing $NADP^+$ as a cofactor, revealed that the carboxylic group of the inhibitory SSA was located at an overlapping position with the 2′-phosphate group of the adenine-side ribose in $NADP^+$ (Fig. 3C). In addition, the results indicated that the binding of the inhibitory SSA in ESS-complex structure brought about a rotational change of

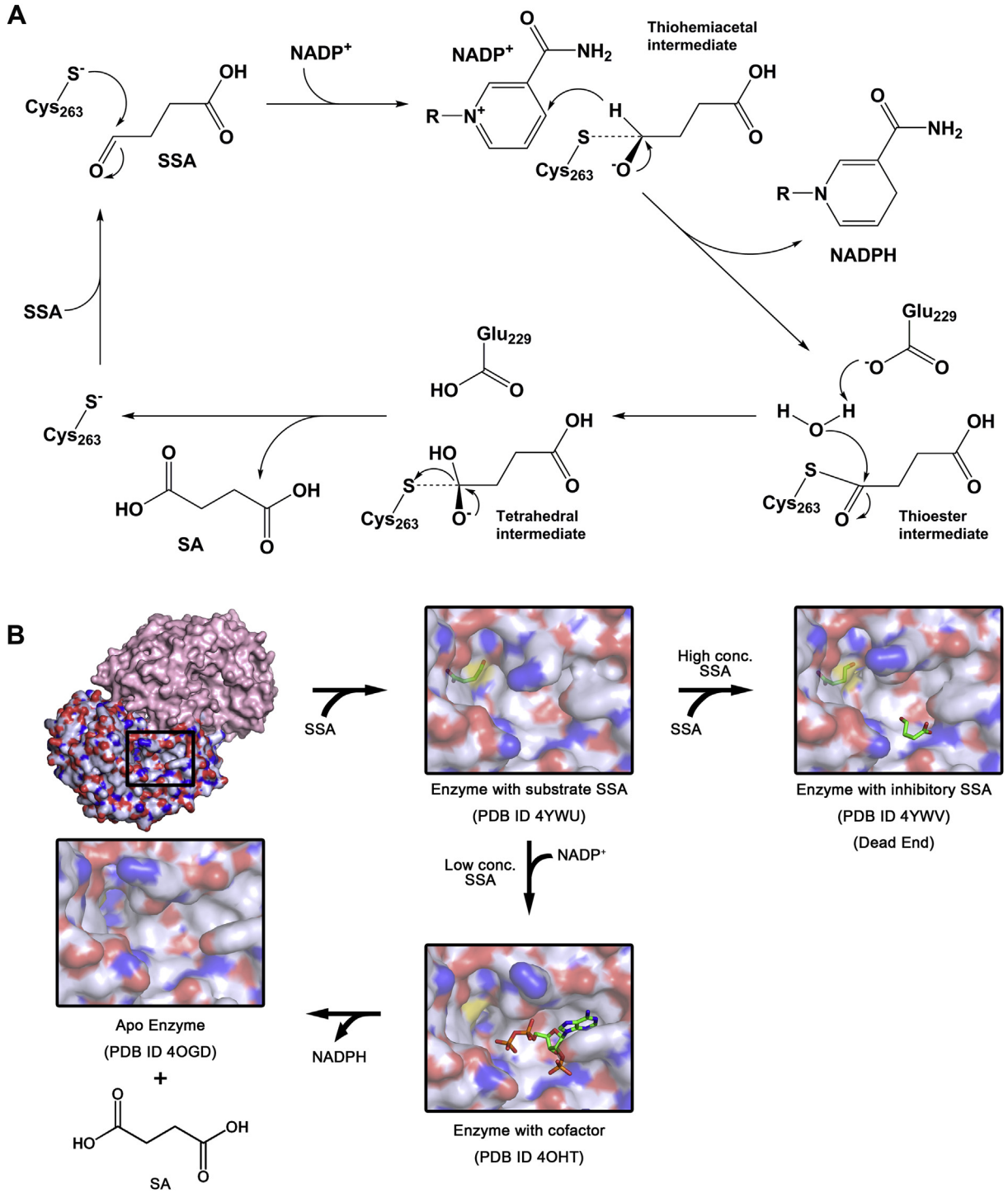

Fig. 4. Proposed catalytic and inhibitory mechanisms of SpSSADH. (A) Proposed catalytic mechanism of SpSSADH. (B) Proposed substrate inhibition model of SpSSADH. The overall structure of SpSSADH is shown as a surface representation (left top). Black boxes show close-up views of the substrate-binding and the cofactor-binding sites of each state.

about 120° in the hydroxyphenyl side chain of Tyr188 residue, which may interfere with the binding of $NADP^+$. Taken together, our results revealed that the substrate inhibition of SpSSADH was induced by the occupation of the cofactor-binding site by additional substrate, away from the active site, as a site of inhibition.

3.4. Proposed catalytic mechanism of SpSSADH

To date, several catalytic mechanisms have been proposed for SSADH, including the following. First, the proposed sequential catalytic mechanism of *Salmonella typhimurium* YneI involves nucleophilic attack by the active site Cys268 (as a cysteine thiolate) at the aldehyde carbonyl group of SSA resulting in the formation of the hemithioacetal tetrahedral intermediate and its subsequent conversion to a thioacyl enzyme intermediate with simultaneous hydride transfer to NAD^+ [9]. Second, another sequential catalytic mechanism was identified in cyanobacterial SSADH. It was suggested that preferential binding of the cofactor to the catalytic cysteine, and speculates that the formation of a cofactor-cysteine adduct may protect the catalytic cysteine from oxidation [23]. Third, from the proposed mechanism of the SSADH from *Mycobacterium tuberculosis*, it was suggested that GabD1 follows a non-rapid equilibrium random kinetic mechanism [3]. In the present study, when the estimated K_m value for the substrate was compared with that for the cofactor, SpSSADH exhibited a high affinity for SSA ($3.95 \pm 0.08 \times 10^{-3}$ mM), which was approximately 25-fold lower than that for $NADP^+$ (0.10 ± 0.01 mM) [12]. Consequently, our results indicate that SpSSADH may adopt the first sequential catalytic mechanism (Fig. 4A), which is consistent with the proposed catalytic mechanism of *S. typhimurium* YneI.

In conclusion, based on the kinetic and structural results, we propose that the substrate inhibition of SpSSADH is caused by the binding of additional substrate, as an inhibitor, to the cofactor-binding site (Fig. 4B). That is, at low concentrations of substrate, SSA and $NADP^+$ are bound to their corresponding positions on SpSSADH, and the catalytic reaction proceeds normally to generate the product SA. However, in the presence of high substrate concentrations, the inhibitory SSA, instead of $NADP^+$, binds to the cofactor-binding site of SpSSADH, through which the catalytic reaction is eventually terminated by the absence of a hydrogen acceptor.

Conflict of interest

None of the authors have any potential conflicts of interest or financial interests to disclose.

Acknowledgments

We would like to thank the staff of beamline 5C at Pohang Accelerator Laboratory in South Korea for assistance during X-ray data collection. This work was supported by a Korea University Grant.

Transparency document

Transparency document related to this article can be found online at http://dx.doi.org/10.1016/j.bbrc.2015.04.047.

References

[1] C. Chen, J.C. Joo, G. Brown, E. Stolnikova, A.S. Halavaty, A. Savchenko, W.F. Anderson, A.F. Yakunin, Structure-based mutational studies of substrate inhibition of betaine aldehyde dehydrogenase BetB from *Staphylococcus aureus*, Appl. Environ. Microbiol. 80 (2014) 3992–4002.
[2] B. Jackson, C. Brocker, D.C. Thompson, W. Black, K. Vasiliou, D.W. Nebert, V. Vasiliou, Update on the aldehyde dehydrogenase gene (ALDH) superfamily, Hum. Genomics 5 (2011) 283–303.
[3] L.P. de Carvalho, Y. Ling, C. Shen, J.D. Warren, K.Y. Rhee, On the chemical mechanism of succinic semialdehyde dehydrogenase (GabD1) from *Mycobacterium tuberculosis*, Arch. Biochem. Biophys. 509 (2011) 90–99.
[4] N. Bouche, H. Fromm, GABA in plants: just a metabolite? Trends Plant Sci. 9 (2004) 110–115.
[5] B.L. Schneider, S. Ruback, A.K. Kiupakis, H. Kasbarian, C. Pybus, L. Reitzer, The *Escherichia coli gabDTPC* operon: specific gamma-aminobutyrate catabolism and nonspecific induction, J. Bacteriol. 184 (2002) 6976–6986.
[6] N. Bouche, A. Fait, D. Bouchez, S.G. Moller, H. Fromm, Mitochondrial succinic-semialdehyde dehydrogenase of the gamma-aminobutyrate shunt is required to restrict levels of reactive oxygen intermediates in plants, Proc. Natl. Acad. Sci. U. S. A. 100 (2003) 6843–6848.
[7] K.J. Kim, P.L. Pearl, K. Jensen, O.C. Snead, P. Malaspina, C. Jakobs, K.M. Gibson, Succinic semialdehyde dehydrogenase: biochemical-molecular-clinical disease mechanisms, redox regulation, and functional significance, Antioxid. Redox. Signal. 15 (2011) 691–718.
[8] T. Fuhrer, L. Chen, U. Sauer, D. Vitkup, Computational prediction and experimental verification of the gene encoding the NAD^+/$NADP^+$-dependent succinate semialdehyde dehydrogenase in *Escherichia coli*, J. Bacteriol. 189 (2007) 8073–8078.
[9] H. Zheng, A. Beliavsky, A. Tchigvintsev, J.S. Brunzelle, G. Brown, R. Flick, E. Evdokimova, Z. Wawrzak, R. Mahadevan, W.F. Anderson, A. Savchenko, A.F. Yakunin, Structure and activity of the $NAD(P)^+$-dependent succinate semialdehyde dehydrogenase YneI from *Salmonella typhimurium*, Proteins 81 (2013) 1031–1041.
[10] R.L. Burton, S. Chen, X.L. Xu, G.A. Grant, A novel mechanism for substrate inhibition in *Mycobacterium tuberculosis* D-3-phosphoglycerate dehydrogenase, J. Biol. Chem. 282 (2007) 31517–31524.
[11] M.C. Reed, A. Lieb, H.F. Nijhout, The biological significance of substrate inhibition: a mechanism with diverse functions, Bioessays 32 (2010) 422–429.
[12] E.H. Jang, S.A. Park, Y.M. Chi, K.S. Lee, Kinetic and structural characterization for cofactor preference of succinic semialdehyde dehydrogenase from *Streptococcus pyogenes*, Mol. Cells 37 (2014) 719–726.
[13] E.H. Jang, J.E. Lim, Y.M. Chi, K.S. Lee, Crystallization and preliminary X-ray crystallographic studies of succinic semialdehyde dehydrogenase from *Streptococcus pyogenes*, Acta Crystallogr. Sect. F. Struct. Biol. Cryst. Commun. 68 (2012) 288–291.
[14] S.K. Wright, R.E. Viola, Evaluation of methods for the quantitation of cysteines in proteins, Anal. Biochem. 265 (1998) 8–14.
[15] S.A. Park, Y.S. Park, K.S. Lee, Kinetic characterization and molecular modeling of $NAD(P)^+$-dependent succinic semialdehyde dehydrogenase from *Bacillus subtilis* as an ortholog YneI, J. Microbiol. Biotechnol. 24 (2014) 954–958.
[16] Z. Otwinowski, W. Minor, Processing of X-ray diffraction data collected in oscillation mode, Methods Enzymol. 276 (1997) 307–326.
[17] P.D. Adams, R.W. Grosse-Kunstleve, L.W. Hung, T.R. Ioerger, A.J. McCoy, N.W. Moriarty, R.J. Read, J.C. Sacchettini, N.K. Sauter, T.C. Terwilliger, PHENIX: building new software for automated crystallographic structure determination, Acta Crystallogr. D. Biol. Crystallogr. 58 (2002) 1948–1954.
[18] A.T. Brunger, P.D. Adams, G.M. Clore, W.L. DeLano, P. Gros, R.W. Grosse-Kunstleve, J.S. Jiang, J. Kuszewski, M. Nilges, N.S. Pannu, R.J. Read, L.M. Rice, T. Simonson, G.L. Warren, Crystallography & NMR system: a new software suite for macromolecular structure determination, Acta Crystallogr. D. Biol. Crystallogr. 54 (1998) 905–921.
[19] P. Emsley, K. Cowtan, Coot: model-building tools for molecular graphics, Acta Crystallogr. D. Biol. Crystallogr. 60 (2004) 2126–2132.
[20] R.A. Laskowski, M.W. MacArthur, D.S. Moss, J.M. Thornton, PROCHECK: a program to check the stereochemical quality of protein structures, J. Appl. Crystallogr. 26 (1993) 283–291.
[21] L.L.C. Schrodinger, The PyMOL Molecular Graphics System, Version 1.3r1, 2010.
[22] J. Dundas, Z. Ouyang, J. Tseng, A. Binkowski, Y. Turpaz, J. Liang, CASTp: computed atlas of surface topography of proteins with structural and topographical mapping of functionally annotated residues, Nucleic Acids Res. 34 (2006) W116–W118.
[23] J. Park, S. Rhee, Structural basis for a cofactor-dependent oxidation protection and catalysis of cyanobacterial succinic semialdehyde dehydrogenase, J. Biol. Chem. 288 (2013) 15760–15770.